Journal of Analytical and Applied Pyrolysis 191 (2025) 107187

Contents lists available at ScienceDirect

Journal of Analytical and Applied Pyrolysis

journal homepage: www.elsevier.com/locate/jaap

Investigation of primary and secondary char formation during pyrolysis of torrefied cellulose

Jinzheng Chen, Zhimin Lu *, Jianfeng Cai, Yulong Lin, Yanjiang Li, Shunchun Yao *

School of Electric Power Engineering, South China University of Technology, Guangzhou 510640, China

ARTICLE INFO

Keywords:
Cellulose
Torrefaction
Pyrolysis
Char formation
Secondary reactions

ABSTRACT

Biomass preparation by torrefaction could be a suitable option to improve the quality of biomass feedstocks for a subsequent thermal conversion process. Char produced from the pyrolysis of torrefied biomass is critical to downstream process development. This study explored the primary and secondary char formation of the torrefied cellulose, with the extent of secondary reaction manipulated by the sample dimension, pyrolysis pressure and pyrolysis heating rate. Cellulose samples were torrefied at 200 °C, 260 °C, and 320 °C, and subsequently pyrolyzed in a hot-plate reactor at 1000 °C, under heating rates of 10–200 °C/min with a pressure of 0.1 or 1000 mbar, using either thin-film or thick-layer samples. The results indicated that the structural transformation induced by torrefaction and the secondary reactions promoted by the pyrolysis conditions led to significant variations in the char yield, ranging from 1.6 wt% to 57.8 wt%. Torrefaction enhanced char formation during the primary reactions in two ways: by reducing the degree of depolymerization of the carbohydrate structure and by promoting the formation of crosslinked structures. The sensitivity of secondary char formation to the pyrolysis conditions varied with torrefaction severity, with the maximum increase in char yield from promoted secondary reactions decreasing as torrefaction severity intensified, ranging from 3.9 to 1.1 times. Raman spectra revealed that the secondary reactions enhanced the condensation of aromatic systems of the char. These findings provide insight into the complex mechanisms underlying primary and secondary char formation during the pyrolysis of torrefied biomass.

1. Introduction

The key strategies for meeting the ambitious targets of the Paris Agreement include carbon capture, storage, and utilization, enhancing energy conservation and efficiency, increasing the use of renewable resources, and deploying negative emissions technologies (NETs) [1]. Bioenergy with carbon capture and sequestration/storage (BECCS) is indispensable to achieving climate targets as it can produce fuels, chemicals, and electricity while reducing atmospheric CO_2 [2]. Maximizing BECCS net carbon and energy balance necessitates the efficient and economical storage, transportation, and processing of substantial quantities of biomass feedstock. Despite the abundant availability of lignocellulosic biomass, its inherent characteristics—such as structural diversity, high moisture content, hydrophilicity, low bulk density, and tough fibrous structure—pose significant challenges to its utilization, making the process complex and costly [3]. Torrefaction, a mild form of pyrolysis, offers a solution to many of these challenges by enhancing the fuel properties of raw biomass [4]. By integrating torrefaction as a pretreatment step in the bioenergy supply chain, it is possible to substantially reduce the costs associated with biomass feedstock storage, transportation, and downstream processing, while simultaneously improving the performance of biomass as a fuel. It has been recognized as a key levers to improve the sustainability of BECCS [5].

Pyrolysis plays a crucial role in the thermochemical utilization of torrefied biomass, not only as a standalone technology for producing value-added chemicals but also as a key sub-process in other thermochemical methods such as gasification and combustion. While these processes differ in reactor configurations, reaction parameters, and target products, char formation during pyrolysis is a common element across them. This char formation process significantly influences both the yield and the properties of char, which, in turn, affects its performance in subsequent applications such as energy production and metallurgy. Torrefaction has been shown to significantly impact char formation during pyrolysis by inducing structural changes in biomass, thereby altering the initiation of the char formation process during pyrolysis [6,7]. The resulting changes in char yield and its properties due

* Correspondence to : School of Electric Power, South China University of Technology, 510640 Guangzhou, China.
E-mail addresses: zhmlu@scut.edu.cn (Z. Lu), epscyao@scut.edu.cn (S. Yao).

https://doi.org/10.1016/j.jaap.2025.107187
Received 6 January 2025; Received in revised form 13 May 2025; Accepted 19 May 2025
Available online 20 May 2025

to torrefaction can influence the following utilization and performance. For example, it can either extend or shorten the char conversion time during combustion or gasification [8,9] and enhance the catalytic performance of biochar in methane reforming [10]. Therefore, understanding char formation during the pyrolysis of torrefied biomass is essential for improving product selectivity and quality.

Biomass feedstocks used in pyrolysis are considerably large, typically in a size range from a few millimeters to several centimeters [11]. Pyrolysis of such large particles is inherently complex, with intraparticle phenomena that intertwine chemical reactions and physical processes [12,13]. In this case, the secondary reactions could not be neglected. During pyrolysis, lignocellulosic biopolymers first undergo degradation to produce primary solid and volatile products, a process known as primary reactions. These primary products are subsequently transformed into char and gas through secondary reactions, with char being regarded as a product of secondary reactions [14]. The secondary char formation involve reactions such as polymerization, crosslinking, and dehydration of condensable volatiles in the liquid phase [15,16], as well as interactions between the volatiles and the solid matrix [17]. The constrained release of permanent gases and condensable fractions from the biomass particle facilitates these secondary reactions, ultimately enhancing char yield. Pecha et al. [18] investigated the nature of secondary reactions in a liquid intermediate, which they proposed a reaction pathway from cellulose to char in a liquid intermediate. Anca-Couce et al. [19] incorporated secondary reactions into the Ranzi scheme and improved the prediction of the final char yield and the yields of the main groups of volatiles. Although the importance of secondary reactions in biomass pyrolysis and their influence on char formation has been recognized, limited attention has distinguished between the primary and secondary reactions in the pyrolysis of torrefied biomass. As torrefaction alters the initial structure of biomass and hence changes the starting material for pyrolysis, understanding the link between the structural transformations from torrefaction and the primary and secondary char formation during pyrolysis is crucial for elucidating char formation mechanisms in torrefied biomass pyrolysis.

Cellulose is a logical starting point for studying the primary and secondary char formation of torrefied biomass because it is the most abundant and simplest polymer in biomass. Moreover, cellulose plays a major role in the increased char yield of torrefied biomass, as its char yield exhibits high sensitivity to torrefaction severity [20,21]. Since secondary reactions are highly related to mass transfer, pyrolysis conditions that affect mass transfer, such as sample dimension [12,22], pyrolysis heating rate [23,24], and pyrolysis pressure [18,25], play an important role in the occurrence of secondary reactions. The adjustments in pyrolysis condition to isolate primary reactions and modulate secondary reactions is of important for investigating primary and secondary char formation of cellulose with different torrefaction severity, a topic currently underexplored and lacking relevant experimental data.

This study aims to investigate primary and secondary char formation during the pyrolysis of torrefied cellulose. The structural transformations in cellulose following torrefaction are characterized using an elemental analyzer, solid-state ^{13}C NMR, XRD, and SEM. To modulate the occurrence of secondary reactions during the pyrolysis, variations in sample dimensions, pyrolysis pressure, and pyrolysis heating rate are applied. The char yields from pyrolysis are then recorded, and the physicochemical structure of the resulting chars is analyzed using elemental analyzer, SEM and Raman spectroscopy. These analyses are conducted to elucidate the nature of the primary and secondary charring behavior in the pyrolysis of torrefied cellulose.

2. Experiments

2.1. Torrefaction pretreatment

Cellulose (Avicel PH-101, Sigma-Aldrich) was torrefied using the method outlined in our previous research [20]. In brief, nitrogen (N_2) gas was introduced into the oven at a flow rate of 1 L/min for 20 min to establish an inert atmosphere prior to heating. Approximately 1 g of cellulose was placed into a porcelain boat, positioned at the center of the preheated oven, and maintained at the set temperature for 60 min. In this study, the torrefaction process was conducted at three different temperatures: 200, 260, and 320 °C. Notably, cellulose entered the pyrolysis stage when heated at 320 °C. This temperature (beyond the traditional torrefaction range of 200–300 °C) was selected to study how severe structural degradation impacts char formation during pyrolysis. For simplicity, each condition was labeled using the first three letters of "cellulose" followed by the respective torrefaction temperature, for example, Cel-200 denotes cellulose torrefied at 200 °C.

The mass yield (Y_m) is defined as Eq. (1) and serves as an indicator of how well the biomass resists thermal degradation [7].

$$Y_m(\%) = \frac{M_T}{M_R} \times 100\% \quad (1)$$

where M_R and M_T are the sample weights before and after torrefaction, respectively.

2.2. Pyrolysis experiment

Before pyrolysis, the raw and torrefied cellulose were first made into thin film and thick layer by a customized quartz plate. The specific production method has been described in detail in previous study [26].

Pyrolysis experiments were conducted using a hot-plate reactor, as described in our previous work [26]. To ensure the accuracy and consistency of the results, each experiment was repeated three times. For vacuum pyrolysis, the prepared sample was placed on the heating platform, and the reactor chamber was sealed. Nitrogen gas (>99.999 % purity) was introduced into the chamber at a flow rate of 1 L/min for 5 min to eliminate air. The vacuum pump was then activated until the internal pressure dropped to 0.1 mbar. Once the desired pressure was achieved, the reactor was heated from room temperature to 1000 °C, with a 10-min hold at the final temperature. A range of heating rates (10, 20, 100, and 200 °C/min) was explored in a parametric study. For atmospheric pressure pyrolysis, nitrogen was introduced for 5 min at a flow rate of 1 L/min, followed by a vacuum stage until the pressure reached 10 mbar. The chamber was then purged with nitrogen, increasing the pressure to approximately 1000 mbar. The sample was heated to 1000 °C at a rate of 10 °C/min, maintaining this temperature for 10 min. After each experiment, the char yield was determined based on the final mass of the char product.

The char yield was calculated using the following equation:

$$Y_C(\%) = \frac{M_{char}}{M_{sample}} \times 100\% \quad (2)$$

where Y_c is the char yield, M_{char} is the weight of the char, and M_{sample} is the weight of the pyrolysis sample.

2.3. Characterization of torrefied cellulose

2.3.1. Elemental analysis

The elemental composition of raw and torrefied cellulose were analyzed using the elemental analyzer (Vario EL cube).

2.3.2. Solid-state CP/MAS ^{13}C NMR spectroscopy

Solid-state nuclear magnetic resonance (NMR) measurements were conducted using a JEOL ECZ-400R/M1 400 MHz spectrometer, equipped with a 3.2 mm HXY magic-angle spinning (MAS) probe (JEOL RESONANCE Inc., Japan). The operating 13 C Larmor frequency was set to 100.53 MHz, and the MAS frequency was automatically regulated at 15 kHz for all experiments. Detailed operation parameters can be seen in the previous study [26]. A significant challenge in interpreting cellulose NMR spectra is the overlap of signals. To address this, spectral

decomposition was performed using the DIMFIT software developed by Massiot et al. [27]. Peak assignments were made by referencing prior studies in the literature [16,28,29]. Several regions of interest (listed in Table S1) were identified to monitor the changes in functional groups during torrefaction. The spectral deconvolution, shown in Figure S1, was carried out using a combination of Gaussian and Lorentzian functions.

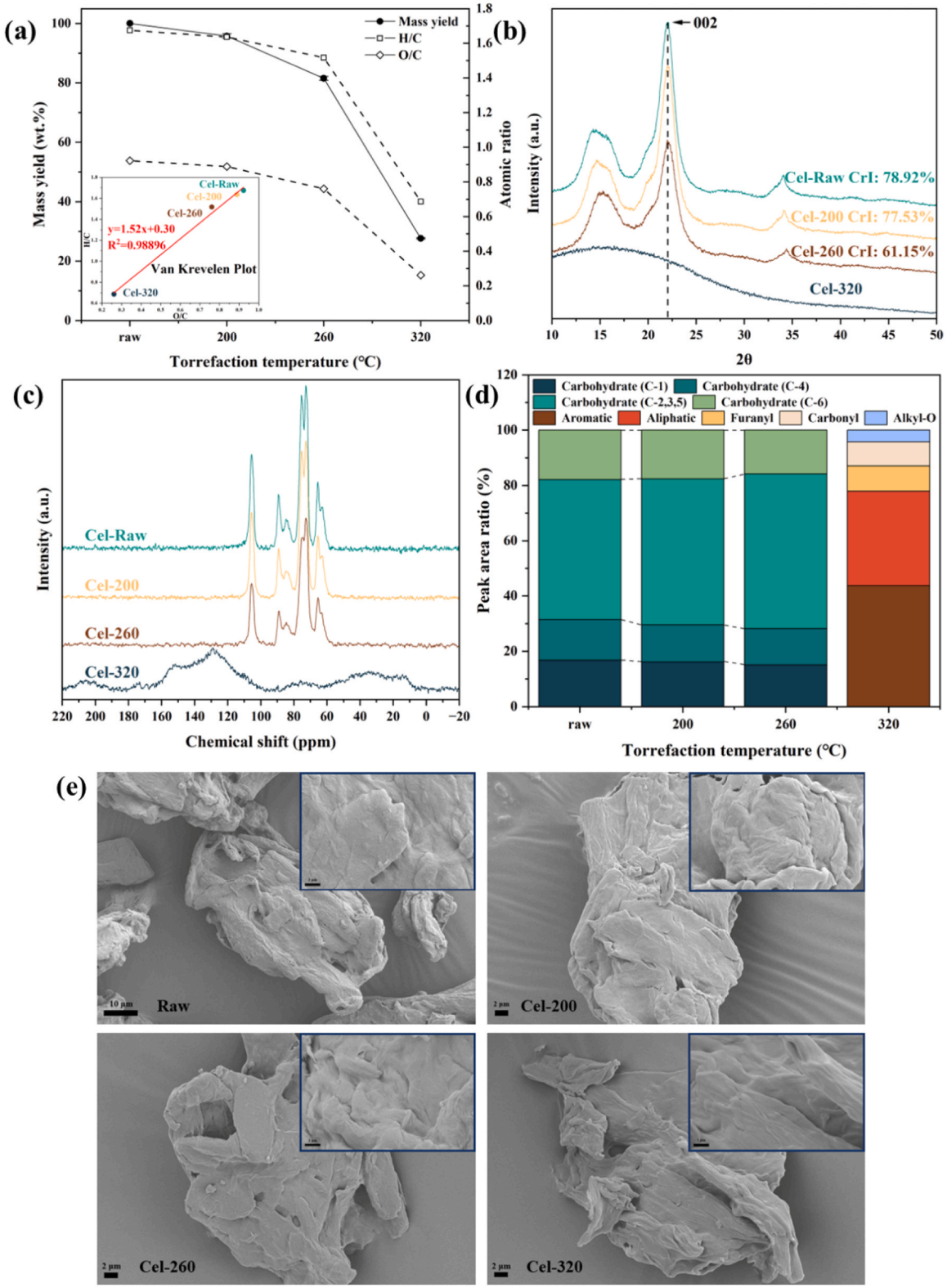

Fig. 1. Mass yield and properties of raw and torrefied cellulose. (a) Mass yields and atomic ratio of cellulose as a function of torrefaction temperature. (b) XRD patterns of the raw and torrefied cellulose. (c) ^{13}C CP/MAS NMR spectra of raw and torrefied cellulose. (d) Functional groups transformation for cellulose torrefied at different temperatures. (e) SEM images of raw and torrefied cellulose.

2.3.3. X-ray diffraction

X-ray diffraction (XRD) analysis was conducted to assess the crystallinity of the char using an Ultima IV X-ray diffractometer. The most prominent peak observed at $2\theta = 22.6°$ was attributed to the crystalline plane 002. The Crystallinity Index (CrI), as defined by Segal et al. [30], was employed to evaluate the crystallinity of both the raw and torrefied cellulose, as described in Eq. (4).

$$CrI(\%) = \frac{I_{002} - I_{am}}{I_{002}} \times 100\% \quad (4)$$

where I_{002} represents the intensity of the 002 diffraction peak intensity, located at the 2θ about 22°, which corresponds to the crystalline region of the sample, and I_{am} refers to the minimum intensity observed at the 2θ around 18°, representing the amorphous component of the material.

2.3.4. Scanning electron microscopy

Surface morphology of the torrefied samples was examined using scanning electron microscopy (SEM, Merlin, Zeiss). To enhance electrical conductivity, all samples were coated with a 3 nm layer of platinum using a Cressington HiRes Sputter Coater. The SEM images were obtained under vacuum conditions with a chamber pressure maintained below 10 mPa. An accelerating voltage of 5 kV was applied for all samples.

2.4. Characterization of pyrolyzed char

Both the physical and chemical properties of the char were analyzed. The elemental analysis and the SEM characterization method is described above. To examine the carbon structural changes in the char samples, Raman spectroscopy (LabRAM Aramis) was performed using a 532 nm laser excitation. The Raman spectra were then deconvoluted using Peakfit 4.0 software.

3. Result and discussion

3.1. Characterization of torrefied cellulose

Fig. 1 illustrates the mass yields and properties of raw and torrefied cellulose. Fig. 1a highlights a downtrend of mass yield at progressively higher torrefaction severity, showing a moderate drop from 100 wt% to 83.32 wt% before 320 °C and a drastic decline at 320 °C which leaves only 27.62 % of the original mass after torrefaction. In tandem with the mass yield, the atomic ratios (O/C and H/C) also gradually decline, which become more pronounced during torrefaction at 320 °C. The variation in the elemental composition of cellulose is well-fitted by a linear function, with a slope of 1.52. The theoretical expectation for pure dehydration, which involves the removal of constitutive water and dehydration of hydroxyl groups during torrefaction, will result in a slope of 2. The slightly lower slope of 1.52 suggests that, in addition to dehydration, a more efficient deoxygenation pathway occurred during torrefaction. This is likely attributed to the release of CO_2 and CO through decarboxylation and decarbonylation reactions [21].

Cellulose is a linear homopolymer made up of repeating cellobiose units, featuring both crystalline and amorphous regions within its structure. The XRD patterns of the raw and torrefied cellulose are shown in Fig. 1b. The crystalline structure of cellulose remains relatively stable when torrefied at 200 °C, with the crystallinity index (CrI) slightly decreasing from 78.92 % in the raw cellulose (Cel-Raw) to 77.53 % in the sample torrefied at 200 °C (Cel-200). However, as the torrefaction temperature increases to 260 °C, the CrI continues to decrease to 61.15 %, indicating a partial conversion of crystalline cellulose into its amorphous form. At 320 °C, the crystalline peaks diminish and eventually become invisible, suggesting that the crystalline structure of cellulose is lost, resulting in the formation of a highly disordered structure in Cel-320 [31].

The ^{13}C NMR spectra of raw and torrefied cellulose, presented in Fig. 1c, reveal two distinct temperature regimes (below and at 320 °C). At torrefaction temperatures of 200 °C and 260 °C, cellulose largely retains its carbohydrate structure. However, at 320 °C, qualitative changes in the NMR spectra become evident, marked by the disappearance of carbohydrate signals and the emergence of significant aromatic and aliphatic signals. Semi-quantitative analyses of the NMR spectra were performed to confirm these qualitative observations. The evolution of signals corresponding to different carbon functional groups is given in Fig. 1d. Below 320 °C, the chemical structure of torrefied cellulose remains largely carbohydrate-based. Within this structure, signals corresponding to C-1, C-4, and C-6 diminish as the torrefaction severity increases. In contrast, the signal for C-2,3,5 gradually intensifies with increasing torrefaction temperature. This pattern may be attributed to inter-chain cleavage within the cellulose, which leads to depolymerization and the formation of anhydrosugars with varying degrees of polymerization [29,32]. At the higher torrefaction temperature of 320 °C, significant structural reorganization occurs, converting the carbohydrate structures into various carbon-functional groups. Aromatic structures become predominant in the cellulose torrefied at 320 °C, with aliphatic, furanyl, carbonyl, and alkyl-O groups also present. These transformations suggest extensive decomposition, dehydration, and crosslinking processes during torrefaction[16].

Fig. 1e presents the SEM pictures of raw cellulose and its torrefied counterparts, and Figure S2 provides a clearer depiction of the surface morphology of raw and torrefied cellulose under high-magnification SEM. The fibrous structure is also observed in Cel-Raw, Cel-200, and Cel-260, indicating only subtle alterations in the cellulose structure at torrefaction temperatures of 200 °C and 260 °C. However, the cellulose torrefied at 260 °C begins to show some differences, with the formation of pores, likely due to mild devolatilization. In contrast, Cel-320 exhibits a complete disappearance of the fibrous structure, which is replaced by a smooth surface. This observation suggests that at 320 °C, cellulose undergoes an intermediate liquid phase, during which severe dehydration and crosslinking reactions occur [20,33].

In summary, cellulose undergoes different transformations at three torrefaction temperatures, as presented in Fig. 2. Cellulose molecules are linear and have a high potential to form both intermolecular and intramolecular hydrogen bonds, resulting in a highly crystalline structure due to the aggregation of linear chains within microfibrils. The physicochemical structure of cellulose torrefied at 200 °C (Cel-200) is similar to that of raw cellulose (Cel-Raw), owing to the inherent thermal stability of cellulose at this temperature. The minimal degradation observed at 200 °C allows Cel-200 to retain the original carbohydrate structure of cellulose largely. Increasing the torrefaction temperature to 260 °C intensifies the degradation of cellulose, leading to the shrinkage of cellulose fibrils and an increase in volatile production. As a result, Cel-260 exhibits a lower degree of polymerization and crystallinity compared to Cel-Raw, though the carbohydrate structure is still preserved. At 320 °C, cellulose undergoes severe transformations. The high torrefaction temperature activates multiple reaction pathways, including glucopyranose ring opening, ring contraction, fragmentation, and dehydration [34], which collectively transform the carbohydrate structure into a crosslinked structure. Consequently, Cel-320 displays a highly heterogeneous carbon structure comprising aromatic, aliphatic, furanyl, carbonyl, and alkyl-O groups.

3.2. Characterization of pyrolyzed char

3.2.1. Char yield

Fig. 3 illustrates the char yields obtained under different pyrolysis conditions in relation to progressive torrefaction temperatures. The char yield follows a consistent trend with increasing torrefaction severity. Initially, the char yield remains constant at a torrefaction temperature of 200 °C, then begins to increase slightly at 260 °C, and finally surges to over 50 wt% when the torrefaction temperature reaches 320 °C. This

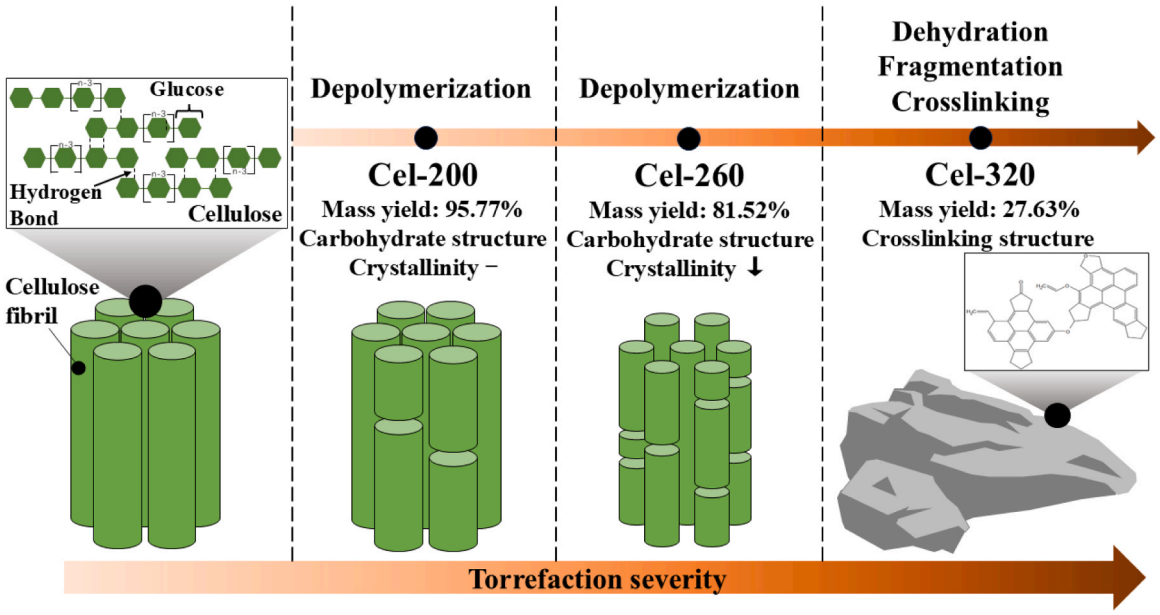

Fig. 2. Schematic diagram of the structural change of cellulose after torrefaction.

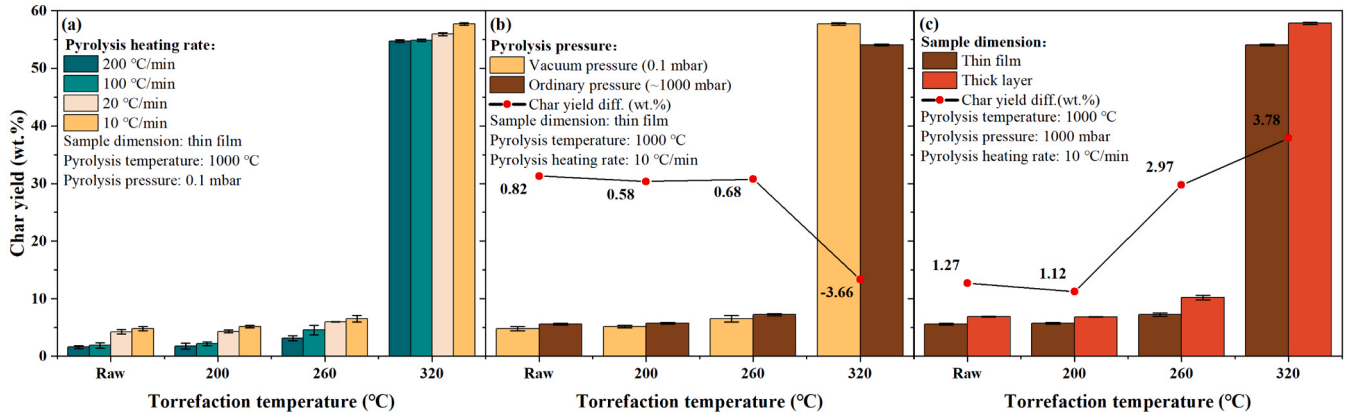

Fig. 3. Char yield of cellulose torrefied at different temperatures: (a) comparison of the effect of pyrolysis heating rate; (b) comparison of the effect of pyrolysis pressure; (c) comparison of the effect of sample dimension.

trend aligns with the structural changes in cellulose at various torrefaction levels: Cel-200 retains a carbohydrate structure like that of Cel-Raw, Cel-260 maintains a carbohydrate structure with a lower degree of polymerization and crystallinity, and in Cel-320, the carbohydrate structure is replaced by a crosslinked structure. The upward trend in char yield with increasing torrefaction severity, observed under conditions that limit secondary reactions (thin film, vacuum pressure, 200 °C/min), suggests that the structural transformations induced by torrefaction promote the primary charring reaction. Furthermore, reducing the heating rate, increasing pyrolysis pressure, and enlarging sample dimensions further boost char formation based on the primary char.

Fig. 3a illustrates the effect of heating rate on the char yield for both raw and torrefied cellulose. Generally, lower heating rates correlate with higher char yields, and this trend is observed in both raw and torrefied cellulose. As heating rate decreases, the char yield consistently increases. Specifically, when the heating rate is reduced from 200 °C/min to 10 °C/min, the char yield increases by 202.7 %, 192.3 %, 110.6 %, and 5.5 % for Cel-Raw, Cel-200, Cel-260, and Cel-320, respectively. This can be attributed to the lower activation energy of dehydration and crosslinking reactions under low heating rates, which favor primary charring reactions and thereby enhance char formation [14,35]. Concurrently, these reactions suppress volatile product generation while enhancing mass transfer limitation. The resulting restricted volatiles transport intensifies secondary reactions, ultimately elevating char yield [23]. In contrast, higher heating rates may shift the reaction pathway toward decomposition, as reactions predominantly occur at higher temperatures. On the one hand, light primary compounds, like furfural, which has a strong polymerization tendency with aromatic compounds at low temperatures [36], can decompose at high temperatures. On the other hand, intensive bond breakage during fast pyrolysis accelerates volatile generation, leading to increased pressure inside the particle, rapid release of volatiles, and a low char yield. Additionally, the influence of heating rate on the char formation diminishes with increasing torrefaction severity. The differences in the physicochemical structure of cellulose at varying levels of torrefaction severity likely account for this observation. As torrefaction alters the cellulose structure, the pathways for char formation change, and these pathways exhibit different sensitivities to heating rates. For Cel-320, the intense devolatilization during torrefaction results in low volatile content, which can reduce the effect of high heating rates on volatile formation. Cel-Raw, Cel-200, and Cel-260, which still contain carbohydrate structures with varying degrees of polymerization and crystallinity, suggest that a reduction in the

degree of polymerization and crystallinity attenuates the impact of heating rate on char formation.

Fig. 3b compares the char yields between vacuum pressure pyrolysis and ordinary pressure pyrolysis, highlighting the influence of pressure on the secondary charring reactions. A slightly higher char yield is observed under ordinary pressure for Cel-Raw, Cel-200, and Cel-260, with increases of 0.8 wt% for Cel-Raw, 0.6 wt% for Cel-200, and 0.7 wt% for Cel-260. Pecha et al. [18] also reported a higher char yield for cellulose under ordinary pressure compared to vacuum conditions. They suggested that vacuum conditions enhance the evaporation of certain heavy primary products of cellulose (e.g., oligosaccharides), thereby reducing dehydration, fragmentation, and crosslinking reactions within the liquid intermediates, which in turn lowers the char yield. However, the impact of pyrolysis pressure seems to be diminished at lower heating rates. At low heating rates, the breaking of weaker chemical bonds favors dehydration and rearrangement reactions, resulting in a more stable matrix [37]. These dehydration and rearrangement reactions, occurring before the onset of depolymerization, reduce the yield of heavy primary products such as oligosaccharides, thereby attenuating the effect of pyrolysis pressure on secondary charring reactions. Unexpectedly, for Cel-320, an increase in pyrolysis pressure decreases the char yield from 57.7 wt% to 54.0 wt%. Repeated experiments verified the reliability of this observation. Additionally, a validation experiment using cellulose from different sources under identical experimental conditions replicated the same trend (as shown in Figure S3 of the supplementary material), that is, elevated pyrolysis pressure does reduce the char yield of Cel-320.

Fig. 3c illustrates the char yields of thin-film and thick-layer cellulose samples as torrefaction temperatures increase. Thick-layer samples consistently show higher char yields compared to thin-film samples, with the disparity in char yield widening as torrefaction severity increases—from 1.1 wt% for Cel-200 to a maximum difference of 3.8 wt % for Cel-320. This increase in char yield is indicative of greater mass transfer resistance in thicker samples, which hinders the release of volatiles and consequently promotes secondary charring reactions [12, 22]. Additionally, the increased char yield of thick-layer cellulose samples can also be attributed to the significant temperature gradients developed within thick-layer cellulose samples during pyrolysis [38]. The lower heat transfer efficiency prolongs low-temperature pyrolysis stages in the interior, thereby promoting primary charring reactions. On the other hand, using a thick layer increases char yield increases of 22.6 %, 19.6 %, 41.0 %, and 7.0 % for Cel-Raw, Cel-200, Cel-260, and Cel-320, respectively. This suggests that the impact of sample thickness on char formation is influenced by torrefaction temperature and the char formation of Cel-260 is the most sensitive to the variation of sample dimension.

It is worth noting that the char yield of raw and torrefied cellulose reaches its peak under the condition that maximize the extent of secondary reactions (i.e., thick layer, atmospheric pressure, and 10 °C/min), with Cel-Raw at 6.9 %, Cel-200 at 6.9 %, Cel-260 at 10.2 %, and Cel-320 at 57.8 %. This condition creates a dual enhancement for char formation. On one hand, the extending duration of low-temperature-pyrolysis stage promotes primary char formation through progressive dehydration of carbohydrate structure within cellulose. On the other hand, the increased mass transfer resistance prolongs volatile-solid matrix interactions to intensify secondary charring reactions. This combined effect ultimately leads to maximized char yields. Compared to the minimum char yield obtained under conditions that suppress secondary reactions (i.e., thin film, vacuum pressure, and 200 °C/min), enhancing secondary reactions increases the char yield by 4.3 times for Cel-Raw, 3.9 times for Cel-200, 3.3 times for Cel-260, and 1.1 times for Cel-320. This trend suggests that as torrefaction severity increases, the influence of pyrolysis conditions on primary and secondary charring reactions weakens, while structural transformations induced by torrefaction become the dominant driver of char formation.

3.2.2. *Physicochemical structure of char*

Elemental compositions of the char samples collected after pyrolysis are presented in the Van Krevelen diagram (Fig. 4). H/C and O/C of the chars derived from raw and torrefied cellulose are located in a narrow range and thus concentrate in a small zone in the Van Krevelen diagram. The influence of the changing torrefied severity and pyrolysis conditions on the char formation is hard to recognize from elemental compositions. Bao et al. [39] reported an insignificant difference in H/C and O/C between cellulose char derived from fast and slow pyrolysis. H/C and O/C are sensitive to the temperature instead of the heating rate.

Although the variations in char chemical structure caused by changing torrefied severity and pyrolysis conditions are unable to be reflected in the Van Krevelen diagram, reaction processes during pyrolysis can be represented by straight lines in the Van Krevelen diagram [40]. After averaging the H/C and O/C of the chars from the same torrefaction-severity cellulose, a linear relationship was built between the raw/torrefied cellulose and the corresponding char. The linear regression equations given in the Van Krevelen diagram exhibit a rising trend of the slope versus increasing torrefaction severity. Given that the slope of the equation should have been 2 when only water evaporation and dehydration reactions occurred during pyrolysis, a growth of the slope from 1.7 for Cel-Raw to 1.9 for Cel-260 indicates the higher torrefaction severity of cellulose, the more intense the dehydration reaction during pyrolysis. Considering the decrease in the degree of polymerization and crystallinity in carbohydrate structure when lifting the torrefaction temperature to 260 °C, it can be concluded that the depolymerization of the carbohydrate structure within cellulose will promote the dehydration reaction. A higher slope of 2.46 can be observed in Cel-320, suggesting that the predominated reaction had shifted from deoxygenation toward dehydrogenation, such as demethylation and demethylenation, along with the condensation of the aromatic ring system [31].

SEM analysis was employed to investigate the morphology of chars, with selected images presented in Fig. 5 for both raw and torrefied cellulose samples. Comprehensive SEM images of all char samples are available in Figure S4 in the Supplementary Material. Notably, porous chars were observed in raw and 200 °C-torrefied cellulose when transformed into thin films and pyrolyzed at a pressure of 0.1 mbar and a heating rate of 200 °C/min, as depicted in Fig. 5a & b. This porous structure aligns with findings reported in the literature [41,42], wherein it is attributed to bubbles formed from liquid boiling during pyrolysis, subsequently leaving pores after the bubble burst. Under identical pyrolysis conditions, the porous structure fades away with increasing

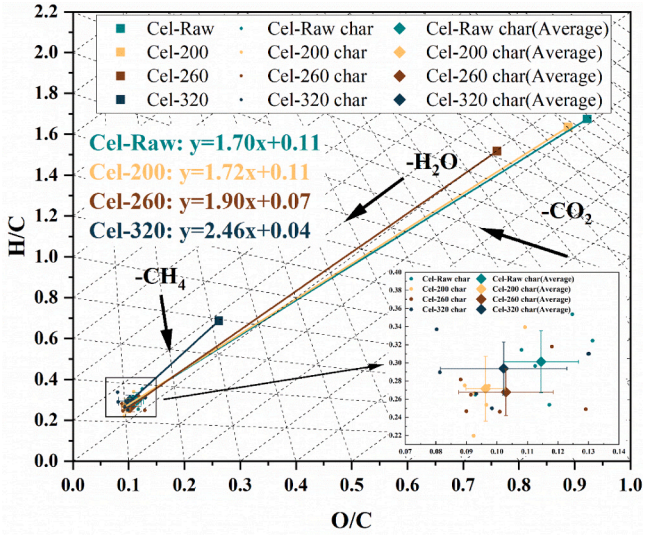

Fig. 4. Van Krevelen diagram for the chars produced from the pyrolysis of raw and torrefied celluloses.

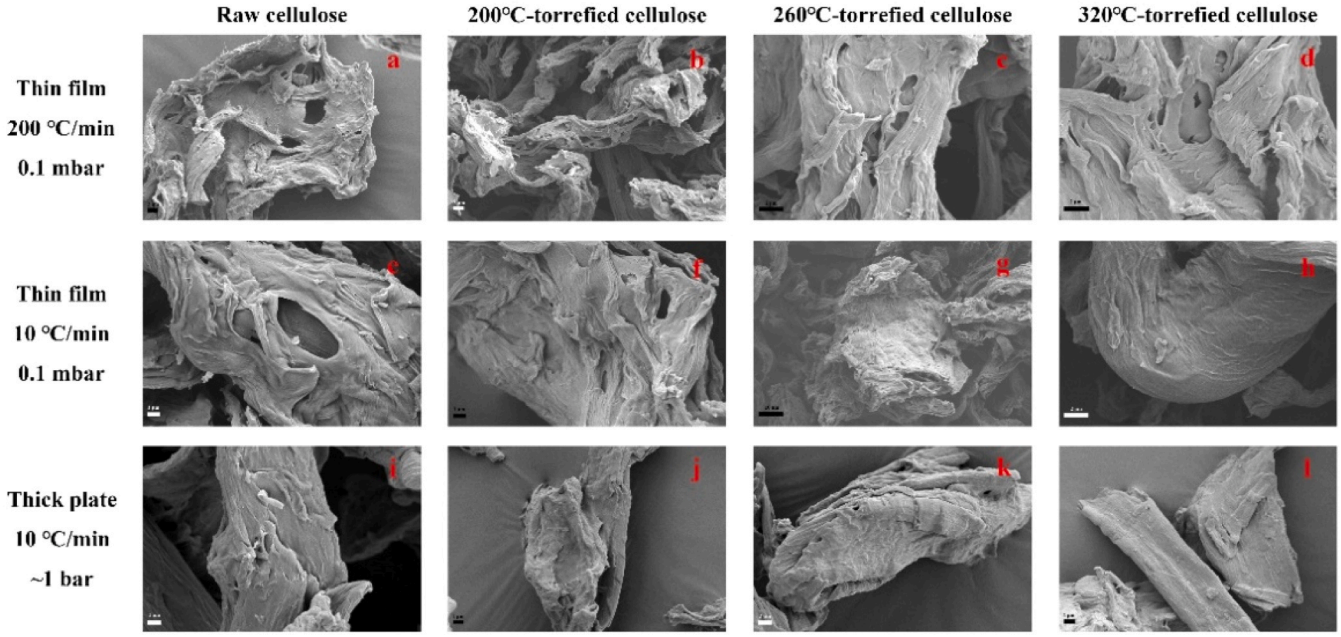

Fig. 5. SEM images of char produced from raw and torrefied cellulose.

torrefaction temperature, reflecting a reduced volatile content after severe torrefaction (see Fig. 5c&d). A similar trend is observed when the heating rate is slowed, indicating a decrease in pore formation with both increasing torrefaction temperature and reduced heating rate. Additionally, elevating pyrolysis pressure and sample thickness further hinders pore formation, developing more consolidated, lumped char structures.

To understand the impact of torrefaction on the carbon structure of char samples, Raman spectroscopy was employed, utilizing the 10-band deconvolution method proposed by Smith et al. [43]. The descriptions of each band and an illustrative example of deconvoluted Raman spectroscopy are provided in Table S2 and Figure S5 in the Supplementary Material, respectively. To track the evolution of the carbon skeletal structure during pyrolysis, we focused on two primary bands associated with the formation of polycyclic aromatic hydrocarbons (PAHs), which are indicative of secondary reactions [12,44]. The D band, which corresponds to larger aromatic ring systems, and the Ds band, associated with smaller aromatic rings, were analyzed [41,43]. The D band region (comprising the S, D_S, D, and A_1 bands) and the G band region (including A_2, G_L, and G_G) are both linked to the development of crystalline or graphite-like carbon structures [31,45]. For clarity, the D and G band regions are labeled as D* and G*, respectively. The area ratios of I_D/I_{Ds}, reflecting the relative amounts of small and large aromatic rings, and I_{D^*}/I_{G^*}, representing the graphite-like carbon structures, were calculated to assess the evolution of the carbon microstructure, as shown in Fig. 6. The pyrolysis conditions in the horizontal coordinate from left to right represent the different degrees of promotion for the secondary reaction.

As depicted in Fig. 6, the I_{D^*}/I_{G^*} of char samples derived from raw and torrefied cellulose at varying pyrolysis conditions fluctuate within a narrow range, averaging 1.45, 1.46, 1.46, and 1.46 for Cel-Raw, Cel-

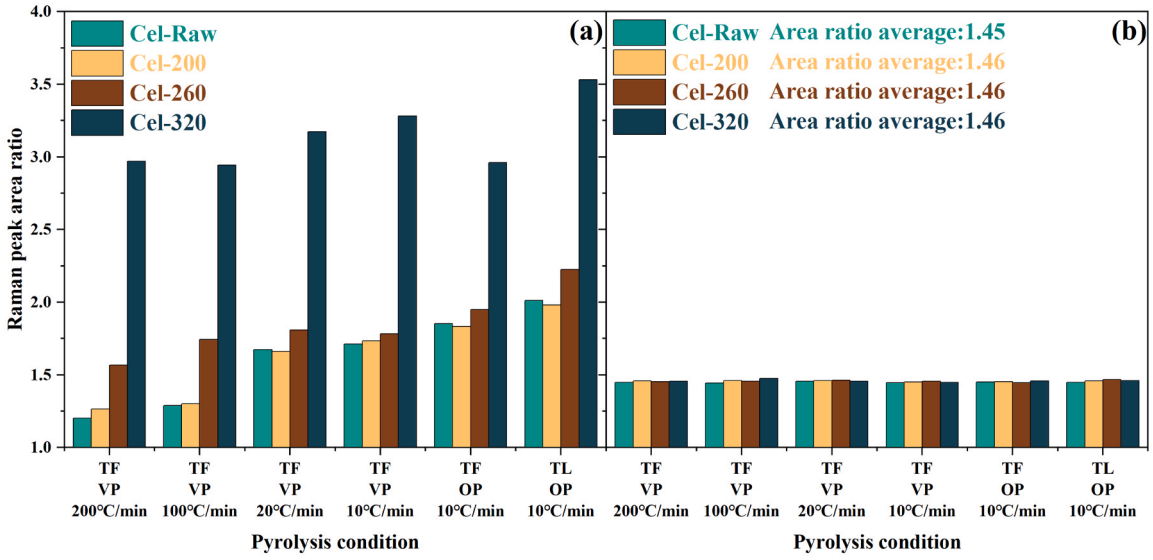

Fig. 6. Carbon structure parameters of char samples from Raman analysis: (a) I_D/I_{Ds}; (b) I_{D^*}/I_{G^*}. The abbreviation TF and TL respectively stand for thin film and thick layer and the abbreviation VP and OP respectively stand for vacuum pressure and ordinary pressure.

200, Cel-260, and Cel-320. This suggests that neither torrefaction severity nor pyrolysis conditions significantly influence the development of graphite-like carbon structures. The high pyrolysis temperature may account for the narrow variation in I_{D*}/I_{G*} values across the samples, as chars produced under high-temperature conditions are generally highly aromatic [31], limiting the sensitivity of I_{D*}/I_{G*} in reflecting subtle differences in carbon structure due to the aforementioned factors. Conversely, the I_D/I_{Ds} values display a broader range, spanning from a minimum of 1.20 to a maximum of 3.53. Below a torrefaction temperature of 320 °C, the I_D/I_{Ds} values consistently increase with the intensification of secondary charring reactions, indicating that these reactions facilitate aromatic nuclei polycondensation and promote the growth of aromatic clusters [46,47]. The chars derived from Cel-320 show higher I_D/I_{Ds} compared with those derived from Cel-Raw, Cel-200, and Cel-260. The higher I_D/I_{Ds} correlates with the crosslinking structure within Cel-320, which favors the formation of a highly condensed aromatic system. It is worth noting that the I_D/I_{Ds} of the char from Cel-320 initially rises from 2.97 to 3.28, then decreases to 2.96, before ultimately increasing again to 3.53 as secondary charring reactions intensify. The reduction in I_D/I_{Ds} in Cel-320 suggests a transformation in char formation by applying ordinary pressure, which restricts the further condensation of the smaller aromatic ring systems.

3.3. Discussion on the primary and secondary charring reaction in the pyrolysis of torrefied cellulose

The experimental results in this study elucidated the combined effect of structural transformation after torrefaction and pyrolysis conditions on the occurrence of secondary charring reaction for torrefied cellulose. The occurrence of the secondary reaction is reflected by evidence in char yield and char structure. The impact of various pyrolysis conditions on the occurrence of the secondary charring reactions displays varying degrees of significance, depending on the severity of torrefaction experienced by the cellulose.

In the case of lightly torrefied cellulose (Cel-200), the original structure is largely preserved due to the inherent thermal stability of cellulose at lower torrefaction temperatures. As a result, Cel-200 exhibits charring behavior similar to raw cellulose. During the primary reaction, Cel-200 initially depolymerizes into liquid intermediates (mainly sugars and anhydro-sugar oligomers). Volatile compounds are either released (depending on the pressure) or remain in the liquid intermediates, continuing to react [18]. Under high heating rate and vacuum conditions, the enhanced thermal ejection and evaporation promote the release of low molecular weight compounds (e.g., acetone and glycolaldehyde) and low-volatility compounds (e.g., levoglucosan and 5-HMF) [48,49]. This limits the secondary reaction within the liquid intermediate, resulting in a low char yield. SEM images in Fig. 5a&b illustrate the formation of a porous structure resulting from the rapid release of volatiles. Slowing down the heating rate lifts the char yield of Cel-200. This can be attributed to greater transport limitations and the lower activation energy of dehydration and crosslinking reactions, which are more favorable at low heating rates, promoting secondary charring reactions and leading to increased char formation [23,35]. Increasing both pyrolysis pressure and sample dimension further enhances char formation, suggesting that the additional transport limitations caused by these factors favor secondary charring reactions, resulting in higher char yields. It is worth noting that the effect of pyrolysis pressure and sample dimension on secondary charring is mild. In contrast, a study by Pecha et al. [18] found that ordinary pressure significantly increased char yield compared to vacuum pressure during the fast pyrolysis (500 °C) of cellulose. Since the present work uses different heating rates and temperatures, it can be concluded that the influence of pyrolysis pressure on secondary charring during the pyrolysis of Cel-Raw and Cel-200 is determined by reaction pathways influenced by the heating rate and temperature.

In the case of mild torrefaction, represented by Cel-260, the sever depolymerization reaction during 260 °C brings about greater structural changes of cellulose and hence results in a different charring reaction pathway compared with Cel-Raw, as evidenced in Fig. 4. The depolymerization of the carbohydrate structure after torrefaction at 260 °C reduces the chain length of the carbohydrate structure. Concurrently, a higher char yield under limiting secondary reaction conditions is found in Cel-260. This suggests that the enhanced primary char yield of Cel-260 is closely linked to the torrefaction-induced reduction in the carbohydrate chain length. Previous studies have shown that reducing the chain length of carbohydrate structures favors char formation during primary reactions [50,51]. Vinu and Broadbelt [50] described the effect of the chain length on cellulose behavior by developing a microkinetic model of glucose-based carbohydrates pyrolysis and emphasized the influence of chain length reduction on promoting the formation of melt phase and changing product distribution. Mettler et al. [51] associated the higher char yield of short-chain carbohydrates with the increased production of 5-HMF, which tends to repolymerize in the intermediate liquid phase, forming char precursors. Although Cel-260 exhibits a higher primary char yield compared to Cel-Raw and Cel-200, the increases in char yield due to reduced heating rate and increased pressure are similar to those observed in Cel-Raw and Cel-200. This implies that for carbohydrate structures, secondary charring reactions—regulated by heating rate and pressure—can retain a comparable mass of carbon-containing compounds in the primary char. However, unlike heating rate and pressure, sample dimension has a more pronounced effect on the secondary charring reaction in Cel-260 compared to Cel-Raw and Cel-200, leading to greater char formation. This indicates that the volatiles generated during Cel-260 pyrolysis have a higher propensity to interact with the carbonaceous matrix when the residence time of volatiles in the reaction zone is prolonged by increasing the sample dimension.

Severely torrefied cellulose, such as that torrefied at 320 °C (Cel-320), undergoes significant physicochemical transformations due to intense degradation, dehydration, and crosslinking during torrefaction [20]. This process transforms the carbohydrate structure into a crosslinking structure, shifting the predominant pyrolysis reactions from deoxygenation toward dehydrogenation and condensation. As a result, the char derived from Cel-320 contains a highly condensed aromatic ring system. This structural shift also weakens bond breakage during pyrolysis, giving Cel-320 an extremely high propensity for char formation, with yields exceeding 50 wt%. The mild devolatilization observed during the pyrolysis of Cel-320 diminishes the effect of transport limitations on secondary charring reactions. Consequently, the char yield increases only slightly with the promotion of secondary reactions through slower heating rates and elevated sample dimension. However, it is noteworthy that increasing pyrolysis pressure actually reduces the char yield of Cel-320. Raman spectroscopy further reveals a reduction in the I_D/I_{Ds} ratio with increased pressure, suggesting that higher pressures may inhibit the polycondensation of smaller aromatic rings into larger ones or potentially induce the consumption of large aromatic structures through self-gasification. While this hypothesis is plausible, it remains speculative, and the exact effect of pyrolysis pressure on char formation during the pyrolysis of Cel-320 warrants further investigation.

Based on the findings of this study and the literature cited herein, a char formation scheme for torrefied cellulose is proposed, as shown in Fig. 7. This scheme is divided into two sub-schemes: one represents the char formation mechanism for mildly torrefied cellulose, such as Cel-200 and Cel-260, which consist predominantly of carbohydrate structures; the other corresponds to severely torrefied cellulose, such as Cel-320, characterized by crosslinked structures. During the pyrolysis of Cel-200 and Cel-260, secondary char formation primarily occurs following the formation of an intermediate liquid phase. The intermediate liquid products and organic volatiles that fail to evaporate or diffuse undergo heterogeneous reactions with the primary char, resulting in crosslinking and polycondensation processes that form secondary char. In contrast, for Cel-320, the crosslinked structure precludes the formation of an

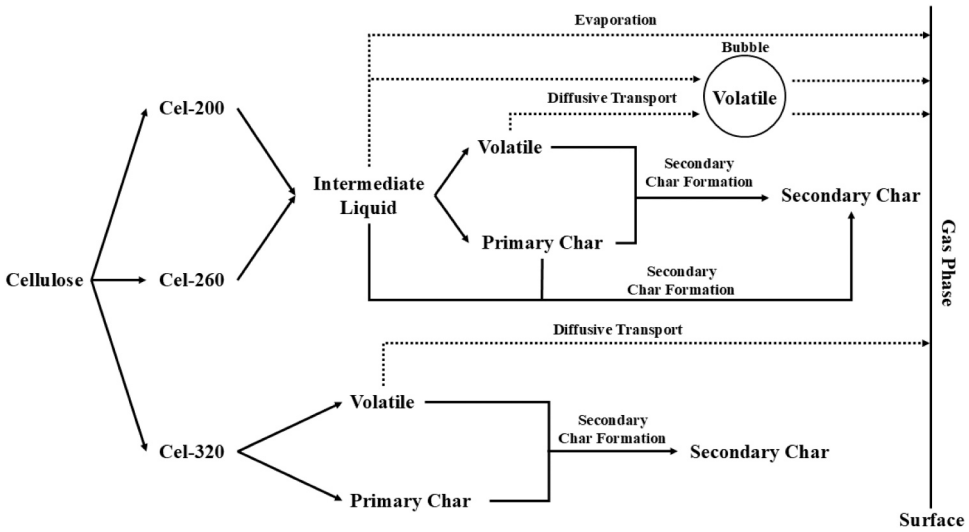

Fig. 7. Char formation scheme during pyrolysis of torrefied cellulose.

intermediate liquid phase during pyrolysis. Instead, secondary char formation arises directly from interactions between volatiles and the primary char.

4. Conclusion

This study investigates the primary and secondary charring behavior during the pyrolysis of raw and torrefied cellulose.The results demonstrate a clear, temperature-dependent transformation of cellulose structure, progressing from a carbohydrate structure to a crosslinked structure. In particular, Cel-200 mostly preserved the original carbohydrate structure of raw cellulose, Cel-260 exhibited a carbohydrate structure with a lower degree of polymerization and crystallinity, while Cel-320 was composed of a crosslinking structure.

The char yield exhibited a significant variation, ranging from 1.6 wt % to 57.8 wt%, depending on the torrefaction severity and pyrolysis conditions. The torrefaction-induced structural transformations promoted the primary char formation during pyrolysis, with primary char yield increasing as torrefaction severity heightened. Furthermore, by adjusting pyrolysis conditions—specifically sample dimension, heating rate, and pressure—the study elucidates how these parameters influence the secondary charring reactions. The findings revealed that the promotion of secondary reactions generally increased char yield, but the sensitivity to pyrolysis conditions varied according to the torrefaction severity of the cellulose. For Cel-200, the heating rate exerted the greatest influence on secondary reactions, whereas the sample dimension had the most pronounced effect on Cel-260. While increasing pressure typically promoted char formation across all samples, a notable exception was Cel-320, where higher pressure led to a decrease in char yield. Moreover, enhancing secondary reactions increases the char yield by 4.3 times for Cel-Raw, 3.9 times for Cel-200, 3.3 times for Cel-260, and 1.1 times for Cel-320, suggesting that the contribution of secondary reactions to char yield diminishes as torrefaction severity increases.

Overall, this study highlights the complex interactions between torrefaction-induced structural transformations and pyrolysis conditions, providing a fundamental understanding of how both structural changes and reaction pathways influence char formation. These findings are crucial for optimizing biomass pretreatment and pyrolysis conditions to enhance char production for various applications.

CRediT authorship contribution statement

Jinzheng Chen: Investigation, Methodology, Data curation, Writing – original draft. **Zhimin Lu:** Conceptualization, Funding acquisition, Supervision, Writing – review and editing. **Jianfeng Cai:** Writing – review and editing. **Yulong Lin:** Writing – review and editing. **Yanjiang Li:** Writing – review and editing. **Shunchun Yao:** Resource, Supervision, Funding acquisition.

Declaration of Competing Interest

The authors declare the following financial interests/personal relationships which may be considered as potential competing interests: Zhimin Lu reports financial support was provided by National Natural Science Foundation of China. Zhimin Lu reports financial support was provided by Ministry of Education of the People's Republic of China. If there are other authors, they declare that they have no known competing financial interests or personal relationships that could have appeared to influence the work reported in this paper.

Acknowledgments

This work was supported by the National Natural Science Foundation of China (52276190), the Fundamental Research Funds for the Central Universities (2022ZFJH004), the Nature Science Foundation of Guangdong Province (2022A1515010741), the Science and Technology Projects in Guangzhou (2024A04J4486), and the Natural Science Foundation of Guangdong Province for Distinguished Youth (2021B1515020071).

Appendix A. Supporting information

Supplementary data associated with this article can be found in the online version at doi:10.1016/j.jaap.2025.107187.

Data availability

Data will be made available on request.

References

[1] S.K. Thengane, S. Bandyopadhyay, Biochar mines: panacea to climate change and energy crisis? Clean. Technol. Environ. Policy 22 (2020) 5–10, https://doi.org/10.1007/s10098-019-01790-1.
[2] S.K. Thengane, K.S. Kung, A. Gomez-Barea, A.F. Ghoniem, Advances in biomass torrefaction: parameters, models, reactors, applications, deployment, and market, Prog. Energy Combust. Sci. 93 (2022) 101040, https://doi.org/10.1016/j.pecs.2022.101040.

[3] W.H. Chen, B.J. Lin, Y.Y. Lin, Y.S. Chu, A.T. Ubando, P.L. Show, et al., Progress in biomass torrefaction: principles, applications and challenges, Prog. Energy Combust. Sci. 82 (2021), https://doi.org/10.1016/j.pecs.2020.100887.

[4] A. Panahi, N. Vorobiev, M. Schiemann, M. Tarakcioglu, M. Delichatsios, Y. A. Levendis, Combustion details of raw and torrefied biomass fuel particles with individually-observed size, shape and mass, Combust. Flame 207 (2019) 327–341, https://doi.org/10.1016/j.combustflame.2019.06.009.

[5] M. Fajardy, N. Mac Dowell, Can BECCS deliver sustainable and resource efficient negative emissions? Energy Environ. Sci. 10 (2017) 1389–1426, https://doi.org/10.1039/c7ee00465f.

[6] S. Zhang, Y. Su, Y. Xiong, H. Zhang, Physicochemical structure and reactivity of char from torrefied rice husk: effects of inorganic species and torrefaction temperature, Fuel 262 (2020), https://doi.org/10.1016/j.fuel.2019.116667.

[7] X. Li, Z. Lu, J. Chen, X. Chen, Y. Jiang, J. Jian, et al., Effect of oxidative torrefaction on high temperature combustion process of wood sphere, Fuel 286 (2021), https://doi.org/10.1016/j.fuel.2020.119379.

[8] Z. Lu, J. Jian, P.A. Jensen, H. Wu, P. Glarborg, Influence of torrefaction on single particle combustion of wood, Energy Fuels 30 (2016) 5772–5778, https://doi.org/10.1021/acs.energyfuels.6b00806.

[9] Q. He, A. Raheem, L. Ding, J. Xu, C. Cheng, G. Yu, Combining wet torrefaction and pyrolysis for woody biochar upgradation and structural modification, Energy Convers. Manag 243 (2021), https://doi.org/10.1016/j.enconman.2021.114383.

[10] X. Zhao, X. Zhou, G. Wang, P. Zhou, W. Wang, Z. Song, Evaluating the effect of torrefaction on the pyrolysis of biomass and the biochar catalytic performance on dry reforming of methane, Renew. Energy 192 (2022) 313–325, https://doi.org/10.1016/j.renene.2022.04.108.

[11] C.L. Williams, T.L. Westover, R.M. Emerson, J.S. Tumuluru, C. Li, Sources of biomass feedstock variability and the potential impact on biofuels production, Bioenergy Res. 9 (2016) 1–14, https://doi.org/10.1007/s12155-015-9694-y.

[12] L. Wang, N. Li, Y. Lu, R. Zhang, Z. Sun, S. Niu, et al., Product distribution from pyrolysis of large biomass particle: effects of intraparticle secondary reactions, Fuel 325 (2022) 124851, https://doi.org/10.1016/j.fuel.2022.124851.

[13] M. Brennan Pecha, J.I.M. Arbelaez, M. Garcia-Perez, F. Chejne, P.N. Ciesielski, Progress in understanding the four dominant intra-particle phenomena of lignocellulose pyrolysis: chemical reactions, heat transfer, mass transfer, and phase change, Green Chem. 21 (2019) 2868–2898, https://doi.org/10.1039/c9gc00585d.

[14] A. Anca-Couce, Reaction mechanisms and multi-scale modelling of lignocellulosic biomass pyrolysis, Prog. Energy Combust. Sci. 53 (2016) 41–79, https://doi.org/10.1016/j.pecs.2015.10.002.

[15] M.S. Mettler, S.H. Mushrif, A.D. Paulsen, A.D. Javadekar, D.G. Vlachos, P. J. Dauenhauer, Revealing pyrolysis chemistry for biofuels production: conversion of cellulose to furans and small oxygenates, Energy Environ. Sci. 5 (2012) 5414–5424, https://doi.org/10.1039/c1ee02743c.

[16] Z. Wang, B. Pecha, R.J.M. Westerhof, S.R.A. Kersten, C.Z. Li, A.G. McDonald, et al., Effect of cellulose crystallinity on solid/liquid phase reactions responsible for the formation of carbonaceous residues during pyrolysis, Ind. Eng. Chem. Res. 53 (2014) 2940–2955, https://doi.org/10.1021/ie4014259.

[17] P.R. Patwardhan, D.L. Dalluge, B.H. Shanks, R.C. Brown, Distinguishing primary and secondary reactions of cellulose pyrolysis, Bioresour. Technol. 102 (2011) 5265–5269, https://doi.org/10.1016/j.biortech.2011.02.018.

[18] M.B. Pecha, J.I. Montoya, F. Chejne, M. Garcia-Perez, Effect of a vacuum on the fast pyrolysis of cellulose: nature of secondary reactions in a liquid intermediate, Ind. Eng. Chem. Res. 56 (2017) 4288–4301, https://doi.org/10.1021/acs.iecr.7b00476.

[19] A. Anca-Couce, R. Mehrabian, R. Scharler, I. Obernberger, Kinetic scheme of biomass pyrolysis considering secondary charring reactions, Energy Convers. Manag 87 (2014) 687–696, https://doi.org/10.1016/j.enconman.2014.07.061.

[20] J. Chen, Z. Lu, J. Jian, Z. Bao, J. Cai, S. Yao, Effect of torrefaction on yield, reactivity and physicochemical properties of pyrolyzed char from three major biomass constituents, J. Anal. Appl. Pyrolysis 173 (2023), https://doi.org/10.1016/j.jaap.2023.106104.

[21] S. Wang, G. Dai, B. Ru, Y. Zhao, X. Wang, G. Xiao, et al., Influence of torrefaction on the characteristics and pyrolysis behavior of cellulose, Energy 120 (2017) 864–871, https://doi.org/10.1016/j.energy.2016.11.135.

[22] J. Yu, X. Liu, M. Millan, A study on pyrolysis of wood of different sizes at various temperatures and pressures, Fuel 342 (2023) 127846, https://doi.org/10.1016/j.fuel.2023.127846.

[23] C.A. Zaror, I.S. Hutchings, D.L. Pyle, H.N. Stiles, R. Kandiyoti, Secondary char formation in the catalytic pyrolysis of biomass, Fuel 64 (1985) 990–994, https://doi.org/10.1016/0016-2361(85)90156-5.

[24] A. Trubetskaya, G. Surup, A. Shapiro, R.B. Bates, Modeling the influence of potassium content and heating rate on biomass pyrolysis, Appl. Energy 194 (2017) 199–211, https://doi.org/10.1016/j.apenergy.2017.03.009.

[25] M.B. Pecha, E. Terrell, J.I. Montoya, F. Stankovikj, L.J. Broadbelt, F. Chejne, et al., Effect of PRessure on Pyrolysis of Milled Wood Lignin and Acid-washed Hybrid Poplar Wood, Ind. Eng. Chem. Res. 56 (2017) 9079–9089, https://doi.org/10.1021/acs.iecr.7b02085.

[26] J. Chen, Z. Lu, Z. Bao, J. Cai, Y. Wei, S. Yao, Char formation during pyrolysis of torrefied cellulose: role of potassium catalysis and torrefaction pretreatment, J. Anal. Appl. Pyrolysis 181 (2024) 106644, https://doi.org/10.1016/j.jaap.2024.106644.

[27] D. Massiot, F. Fayon, M. Capron, I. King, S. Le Calvé, B. Alonso, et al., Modelling one- and two-dimensional solid-state NMR spectra, Magn. Reson Chem. 40 (2002) 70–76, https://doi.org/10.1002/mrc.984.

[28] I. Pastorova, R.E. Botto, P.W. Arisz, J.J. Boon, Cellulose char structure: a combined analytical Py-GC-MS, FTIR, and NMR study, Carbohydr. Res 262 (1994) 27–47, https://doi.org/10.1016/0008-6215(94)84003-2.

[29] Y. Le Brech, J. Raya, L. Delmotte, N. Brosse, R. Gadiou, A. Dufour, Characterization of biomass char formation investigated by advanced solid state NMR, Carbon N. Y 108 (2016) 165–177, https://doi.org/10.1016/j.carbon.2016.06.033.

[30] L. Segal, J.J. Creely, A.E. Martin, C.M. Conrad, An empirical method for estimating the degree of crystallinity of native cellulose using the x-ray diffractometer, Text. Res J. 29 (1959) 786–794.

[31] S. Xin, H. Yang, Y. Chen, M. Yang, L. Chen, X. Wang, et al., Chemical structure evolution of char during the pyrolysis of cellulose, J. Anal. Appl. Pyrolysis 116 (2015) 263–271, https://doi.org/10.1016/j.jaap.2015.09.002.

[32] T. Melkior, S. Jacob, G. Gerbaud, S. Hediger, L. Le Pape, L. Bonnefois, et al., NMR analysis of the transformation of wood constituents by torrefaction, Fuel 92 (2012) 271–280, https://doi.org/10.1016/j.fuel.2011.06.042.

[33] D. Liu, Y. Yu, H. Wu, Evolution of water-soluble and water-insoluble portions in the solid products from fast pyrolysis of amorphous cellulose, Ind. Eng. Chem. Res 52 (2013) 12785–12793, https://doi.org/10.1021/ie401806y.

[34] V. Agarwal, P.J. Dauenhauer, G.W. Huber, S.M. Auerbach, Ab initio dynamics of cellulose pyrolysis: nascent decomposition pathways at 327 and 600 °c, J. Am. Chem. Soc. 134 (2012) 14958–14972, https://doi.org/10.1021/ja305135u.

[35] V. Mamleev, S. Bourbigot, M. Le Bras, J. Yvon, The facts and hypotheses relating to the phenomenological model of cellulose pyrolysis. Interdependence of the steps, J. Anal. Appl. Pyrolysis 84 (2009) 1–17, https://doi.org/10.1016/j.jaap.2008.10.014.

[36] X. Hu, Y. Wang, D. Mourant, R. Gunawan, C. Lievens, W. Chaiwat, et al., Polymerization on heating up of bio-oil: a model compound study, AIChE J. 59 (2013) 888–900, https://doi.org/10.1002/aic.13857.

[37] F.X. Collard, J. Blin, A review on pyrolysis of biomass constituents: mechanisms and composition of the products obtained from the conversion of cellulose, hemicelluloses and lignin, Renew. Sustain Energy Rev. 38 (2014) 594–608, https://doi.org/10.1016/j.rser.2014.06.013.

[38] M.M. Hasan, X. Hu, R. Gunawan, C.Z. Li, Pyrolysis of large mallee wood particles: Temperature gradients within a pyrolysing particle and effects of moisture content, Fuel Process Technol. 158 (2017) 163–171, https://doi.org/10.1016/j.fuproc.2016.12.018.

[39] Z. Bao, Z. Lu, J. Chen, J. Cai, S. Guo, S. Yao, Relationships between char reactivity and char structure from a suite of organic model compounds, Fuel Process Technol. 249 (2023) 107852, https://doi.org/10.1016/j.fuproc.2023.107852.

[40] D.C. Palacio Lozano, H.E. Jones, T. Ramirez Reina, R. Volpe, M.P. Barrow, Unlocking the potential of biofuels: via reaction pathways in van Krevelen diagrams, Green Chem. 23 (2021) 8949–8963, https://doi.org/10.1039/d1gc01796a.

[41] M.W. Smith, B. Pecha, G. Helms, L. Scudiero, M. Garcia-Perez, Chemical and morphological evaluation of chars produced from primary biomass constituents: Cellulose, xylan, and lignin, Biomass Bioenergy 104 (2017) 17–35, https://doi.org/10.1016/j.biombioe.2017.05.015.

[42] D. Magalhães, K. Gürel, L. Matsakas, P. Christakopoulos, I. Pisano, J.J. Leahy, et al., Prediction of yields and composition of char from fast pyrolysis of commercial lignocellulosic materials, organosolv fractionated and torrefied olive stones, Fuel 289 (2021), https://doi.org/10.1016/j.fuel.2020.119862.

[43] M.W. Smith, I. Dallmeyer, T.J. Johnson, C.S. Brauer, J.S. McEwen, J.F. Espinal, et al., Structural analysis of char by Raman spectroscopy: improving band assignments through computational calculations from first principles, Carbon N. Y 100 (2016) 678–692, https://doi.org/10.1016/j.carbon.2016.01.031.

[44] K. Yang, J. Wang, J. Huang, J. Yang, Y. Pan, M. Xu, et al., Understanding the homogeneous reactions of primary tar from biomass pyrolysis by means of photoionization mass spectrometry, Energy Fuels 34 (2020) 12678–12687, https://doi.org/10.1021/acs.energyfuels.0c02178.

[45] D.M. Keown, X. Li, J.I. Hayashi, C.Z. Li, Characterization of the structural features of char from the pyrolysis of cane trash using Fourier transform-Raman spectroscopy, Energy Fuels 21 (2007) 1816–1821, https://doi.org/10.1021/ef070049r.

[46] M. Safar, B.J. Lin, W.H. Chen, D. Langauer, J.S. Chang, H. Raclavska, et al., Catalytic effects of potassium on biomass pyrolysis, combustion and torrefaction, Appl. Energy 235 (2019) 346–355, https://doi.org/10.1016/j.apenergy.2018.10.065.

[47] M. Xia, Z. Chen, Y. Chen, H. Yang, W. Chen, H. Chen, Effect of various potassium agents on product distributions and biochar carbon sequestration of biomass pyrolysis, Energy 289 (2024) 130012, https://doi.org/10.1016/j.energy.2023.130012.

[48] J. Zhang, M.W. Nolte, B.H. Shanks, Investigation of primary reactions and secondary effects from the pyrolysis of different celluloses, ACS Sustain Chem. Eng. 2 (2014) 2820–2830, https://doi.org/10.1021/sc500592v.

[49] A.R. Teixeira, K.G. Mooney, J.S. Kruger, C.L. Williams, W.J. Suszynski, L. D. Schmidt, et al., Aerosol generation by reactive boiling ejection of molten cellulose, Energy Environ. Sci. 4 (2011) 4306–4321, https://doi.org/10.1039/c1ee01876k.

[50] R. Vinu, L.J. Broadbelt, A mechanistic model of fast pyrolysis of glucose-based carbohydrates to predict bio-oil composition, Energy Environ. Sci. 5 (2012) 9808–9826, https://doi.org/10.1039/c2ee22784c.

[51] M.S. Mettler, A.D. Paulsen, D.G. Vlachos, P.J. Dauenhauer, The chain length effect in pyrolysis: bridging the gap between glucose and cellulose, Green Chem. 14 (2012) 1284–1288, https://doi.org/10.1039/c2gc35184f.